

Microstructure evolution of Al-Si-10Mg in direct metal laser sintering using phase-field modeling

Jyotirmoy Nandy¹ · Hrushikesh Sarangi¹ · Seshadev Sahoo¹

Received: 2 March 2017 / Accepted: 15 January 2018 / Published online: 27 February 2018
© Shanghai University and Springer-Verlag GmbH Germany, part of Springer Nature 2018

Abstract Direct metal laser sintering (DMLS) has evolved as a popular technique in additive manufacturing, which produces metallic parts layer-by-layer by the application of laser power. DMLS is a rapid manufacturing process, and the properties of the build material depend on the sintering mechanism as well as the microstructure of the build material. Thus, the prediction of part microstructures during the process may be a key factor for process optimization. In addition, the process parameters play a crucial role in the microstructure evolution, and need to be controlled effectively. In this study, the microstructure evolution of Al-Si-10Mg alloy in DMLS process is studied with the help of the phase field modeling. A MATLAB code is used to solve the phase field equations, where the simulation parameters include temperature gradient, laser power and scan speed. From the simulation result, it is found that the temperature gradient plays a significant role in the evolution of microstructure with different process parameters. In a single-seed simulation, the growth of the dendritic structure increases with the increase in the temperature gradient. When considering multiple seeds, the increasing in temperature gradients leads to the formation of finer dendrites; however, with increasing time, the dendrites join and grain growth are seen to be controlled at the interface.

Keywords Additive manufacturing · Direct metal laser sintering (DMLS) · Phase field modeling · Microstructure

1 Introduction

Additive manufacturing has emerged as an excellent manufacturing technique in recent years. With a vast array of processes falling under the umbrella of additive manufacturing, this class of highly efficient manufacturing methods has now grown over many fields of science and technology, making an enormous impact on different areas of human activity. The layer-by-layer deposition of materials using precise design techniques and high-power energy inputs such as lasers and electron beams has pushed manufacturing techniques in a new direction [1]. From medical applications to the aerospace industry, academic research, and the automobile manufacturing industry, it has found a wide range of applications. Previously confined to the laboratory, now, after decades of study, it is being used successfully in many industries with excellent results [2].

Among the different types of additive manufacturing processes, direct metal laser sintering (DMLS) is a new technique, which produces metallic build parts in a layer-by-layer fashion. A movable, high-energy laser beam scans the powder layer and sinters the powdered material on the substrate layer after layer, producing high density build parts [3–5]. A schematic diagram of the DMLS process is shown in Fig. 1. DMLS is able to produce high density alloys owing to highly specific design and high-power laser input. It is a rapid manufacturing process and the sintering rate is very high. The process has a high degree of design freedom, as part-specific tooling and support structures are not necessary [6, 7]. The high-performance Al-Si-10Mg alloy has good casting properties, which enables the production of cast parts with thin wall geometry and complex designs. The combination of this alloy with DMLS therefore has a very profound advantage. Owing to the good

✉ Seshadev Sahoo
seshadevsahoo@soa.ac.in

¹ Department of Mechanical Engineering, Institute of Technical Education and Research, Siksha 'O' Anusandhan, Bhubaneswar, Odisha 751030, India

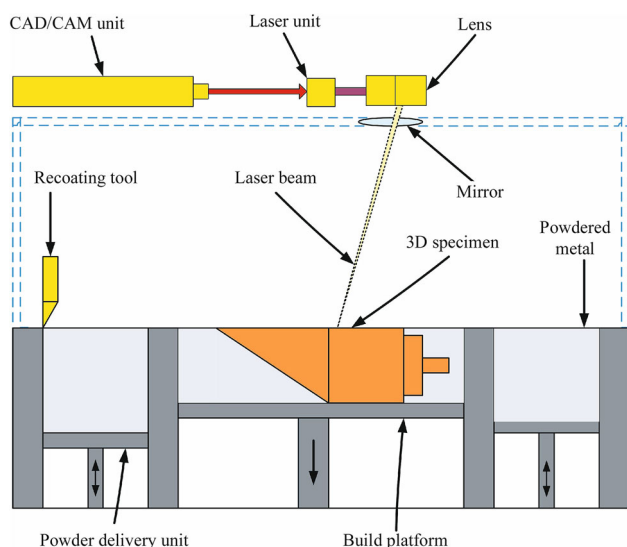


Fig. 1 Schematic diagram of the DMLS process

casting properties of Al-Si-10Mg and the layer-by-layer building process, the parts typically incorporate some amount of anisotropy, which can be changed or eliminated with heat treatment processes [8].

The mechanical properties that are strongly influenced by a materials' microstructure are strength, ductility, and hardness. The evolution of the microstructure determines the final properties and qualities of manufactured materials. These are further controlled by the process parameters such as scan speed, laser power, hatch spacing, hatch pattern, and many others. Controlling these parameters during an experiment is very difficult due to the fast sintering mechanism. These process parameters have a high impact on microstructure formation, which then influences the physical and mechanical properties of the build parts. To control the process parameters during the experiment, a microstructure model is indispensable. Over the past few decades, many approaches have been developed to model the microstructure. Sharp interface modeling and phase-field modeling have been used to simulate microstructure evolution. Phase-field modeling has emerged as a more profound and efficient tool to model the microstructure owing to its enhanced tracking of the microstructure evolution at the interfacial regions [9, 10]. It has been used to simulate many different phenomena such as solidification, martensitic transformations and grain growth, precipitate growth and coarsening, and various solid-state transformations including crack propagation [11–14].

Gránásy et al. [15] studied the formation of polycrystalline growth morphologies with dendrites, grain boundary dynamics, heterogeneous nucleation, particle-front interactions and solidification in confined geometries using

the phase field method. Ganeriwala and Zohdi [16] created a model describing microstructure evolution by using a discrete element approach. In this case, the physical interactions between particles were linked with the mechanical and thermal interactions. Sahoo et al. [17, 18] created a quantitative phase field model to simulate the microstructural changes in a Ti alloy during electron beam additive manufacturing. This study showed that temperature gradients played a significant role in microstructure evolution during the process. Karma [19] studied microstructural pattern formation in alloys using the thin interface limit, which yielded a less severe constraint on the selection of interface thicknesses and allowed the elimination of non-equilibrium effects at the interfaces. Further dendritic growth simulations showed that both the interface evolution and solute profile in the solid were modeled accurately. Tan et al. [20] used both cellular automata and phase-field methods to predict the dendritic growth of multicomponent and multiphase alloys during solidification. Most of the previous work was concerned with modeling the formation of one single crystal from the melt. Fallah et al. [21] modeled the microstructure evolution of a Ti-Nb alloy during a laser deposition process using a phase-field model. They used temperature gradients and the solidification velocity to simulate dendritic growth. Gong and Chou [22] studied the microstructure evolution of Ti-6Al-4V during selective electron beam melting at different amounts of under cooling, and at different speeds. They found that dendrite growth was faster at high under cooling. Biswas et al. [23] adopted a phase-field model to predict the consolidation kinetics during sintering. It was observed that the interactions among the powder particles were initiated due to surface diffusion. Further, densification was primarily governed by volume and grain boundary diffusion. The grains increased in size under pressure until they collided, and the grain boundaries diffused.

Holfelder et al. [24] while studying the microstructure evolution in selective laser melting (SLM), described a multiphase field model. The model was based on the free enthalpy and the nucleation was studied during the phase transformations. Using the alloy Ti-6Al-4V, special attention was given to the transition between β -titanium and the melt. Hang and Mastorakos [25] established that a phase field model of crystal growth could be used to predict the microstructure evolution of metals with a body-centered cubic cell structure during solidification. The study reported a columnar grain structure, which was similar to the grain growth exhibited in real samples produced by additive manufacturing. Kundin et al. [26] presented a model for binary and multi-component systems, and validated it with the help of a steady state Kurz-Fisher model. Phase-field simulations were used to assess

the dependence of growth velocity on under-cooling during the solidification of Inconel 718 alloy using SLM. Furthermore, the study showed the usage of simulated structures and concentration fields as inputs for the precipitation of secondary phases.

To date, no descriptive studies of microstructure modeling in a DMLS process with Al-Si-10Mg have been published. In the present study, phase-field modeling of microstructure evolution of Al-Si-10Mg in a DMLS process is performed by considering a single particle as well as a multi particle system. Out of the three different sintering phenomena affecting microstructure evolution during DMLS, this study mainly focuses on full melting by observing grain growth in the multi-particle domain.

2 Phase field formulation

The phase field method is chosen to model the microstructure evolution of Al-Si-10Mg during a DMLS process. A phase field model is developed to examine the behavior of the phase field variables in the domain using the governing equations. The rapid changes in the interface cause a brisk disturbance in the smooth behavior of the interface. The assumptions made to construct this phase field model are as

- (i) The thermo-physical properties are taken as constants.
- (ii) The latent heat of the system is ignored.
- (iii) The temperature field is replaced by the temperature gradient.
- (iv) The constant temperature term is represented using a temperature that changes with time and position, i.e., $T \rightarrow T_c(x, t)$ where x is the position vector and t is time, to make the system non-isothermal.
- (v) The solid-liquid interface is taken to be in local equilibrium.

Using the conserved and non-conserved phase field variables, the governing equations for the anisotropic phase field term are given as

$$\begin{aligned} \tau A^2(\varphi) \frac{\partial \varphi}{\partial t} &= W_\varphi^2 \nabla(A^2(\varphi) \nabla \varphi) - W_\varphi^2 \partial_x(A(\varphi) A'(\varphi) \partial_y \varphi) \\ &+ W_\varphi^2 \partial_y(A(\varphi) A'(\varphi) \partial_x \varphi) - \frac{d g(\varphi)}{d \varphi} \\ &- \frac{L(T_c - T_m)}{H T_m} \frac{d \rho(\varphi)}{d \varphi} + \eta'(x, T_c), \end{aligned} \tag{1}$$

$$\frac{\partial T}{\partial t} = \nabla(\alpha(\varphi) \nabla T) + \frac{L h'(\varphi)}{C_p} \frac{\partial \varphi}{\partial t}, \tag{2}$$

where τ is the time scale, φ order parameter, $A(\varphi)$ anisotropy parameter, $A'(\varphi)$ derivative of $A(\varphi)$ with respect to the order parameter, W_φ length scale, L latent heat of fusion, T_m melting temperature, T_c critical temperature, H nucleation barrier, $\eta'(x, T_c)$ stochastic noise function emulating thermal fluctuations, $\alpha = k/\rho C_p$ the thermal diffusion coefficient, $h'(\varphi)$ smooth derivative function with limits $h(0) = 0$ and $h(1) = 1$, C_p the specific heat capacity at constant pressure.

By rescaling space and time as $(\bar{x} \rightarrow x/W_\varphi)$ and $(\bar{t} \rightarrow t/\tau)$, we get

$$\begin{aligned} \varphi^{n+1} &= \varphi^n + \frac{\Delta \bar{t}}{A^2(\varphi)} (\nabla(A^2(\varphi) \nabla \varphi - \partial_{\bar{x}}(A(\varphi) A'(\varphi) \partial_{\bar{y}} \varphi) \\ &+ \partial_{\bar{y}}(A(\varphi) A'(\varphi) \partial_{\bar{x}} \varphi)) - \frac{d g(\varphi)}{d \varphi} \\ &- \bar{\lambda} H \frac{d P(\varphi)}{d \varphi} + \eta'(x, T_c)), \end{aligned} \tag{3}$$

$$H^{n+1} = H^n + \frac{\bar{D} \Delta \bar{t}}{\nabla^2 \bar{x}} \Delta^2 H^n + \Delta \bar{t} h'(\varphi^n) \left(\frac{\varphi^{n+1} - \varphi^n}{\Delta \bar{t}} \right), \tag{4}$$

where $\bar{D} = a_2 \bar{\lambda}$, a_2 a constant, and $\bar{\lambda}$ a rescaled λ .

In the current phase field model, the anisotropy effects are included as given in the following equation

$$A(\varphi) = 1 - 3\varepsilon_4 + 4\varepsilon_4 \frac{\left(\frac{\partial \varphi}{\partial x}\right)^4 + \left(\frac{\partial \varphi}{\partial y}\right)^4}{|\nabla \varphi|^4}, \tag{5}$$

where ε_4 is the degree of anisotropy of the surface tension.

As mentioned in the assumptions, the temperature field was introduced in the form of the temperature gradient.

3 Numerical procedure for phase field formulation

For microstructure simulation, a thermal simulation was carried out and the temperature gradient was extracted from the thermal model and incorporated into the phase field equations. Keeping the zero-flux boundary condition, the finite difference method using a central difference scheme was implemented for solving the phase-field equations. The phase-field equations were solved by using a MATLAB code. The top layer of the powder bed was taken to be an X - Y plane. In this case, the flux affects the topmost surface and microstructure evolution occurs in this plane. The domain size was taken to be $500 \mu\text{m} \times 500 \mu\text{m}$ with a grid spacing of $0.03 \mu\text{m}$ in both axes. The simulations were initialized with a circular seed of radius $10 \mu\text{m}$ at the center of the domain, and then, three more circular seeds of radius $10 \mu\text{m}$ each were placed arbitrarily inside the domain.

The computational simulations were performed using the following steps:

- (i) The initial parameters are computed and the phase field is defined in the domain.
- (ii) Order parameters are prepared, and the adaptive mesh refinement is used by pre-allocating the matrices.
- (iii) Anisotropy functions of the order parameters are assigned, and they are differentiated again. The boundary conditions are fixed.
- (iv) The temperature field is set up with the order parameters and they are differentiated.
- (v) The phase field equations are solved using the finite difference method using a central difference scheme.
- (vi) Boundary conditions are applied to the temperature field and noise is introduced in the field.
- (vii) The phase field and the temperature field values are updated, and the simulation repeats steps (iii) and (iv) for successive iterations.

4 Results and discussion

Among the various process parameters such as solidification growth rate, cooling rate, chemical composition, and undercooling, the temperature gradient plays a very specific role in the evolution of the microstructure. The thermo-physical properties of Al-Si-10Mg and the process parameters used in the phase field simulations are given in Tables 1 and 2. The heat flux from the laser beam affects the top surface of the powder layer as well as the substrate. To illustrate the temperature gradient on the top surface of the powder layer with respect to the substrate, a 2D view of the temperature distribution on the powder layer as well as the substrate for a scanning speed of 500 mm/s in the DMLS process is shown in Fig. 2. Based on the thermal profile, the average temperature gradient in the molten pool is calculated. The temperature gradient was calculated based on the equation

Table 1 Thermo-physical properties of Al-Si-10Mg Alloy

Properties	Values
Thermal conductivity $K/(W \cdot (m \cdot K)^{-1})$	113
Specific heat capacity $C_p/(J \cdot (kg \cdot K)^{-1})$	940
Convective heat transfer coefficient $h/(W \cdot (m^2 \cdot K)^{-1})$	80
Density $\rho/(g \cdot m^{-3})$	2.67
Emissivity ε	0.19
Solidus temperature T_s/K	830
Liquidus temperature T_l/K	869

Table 2 Process parameters used for DMLS process

Parameters	Values
Laser power/W	130, 150, 170
Scanning speed/(mm·s ⁻¹)	500, 750, 1 000
Laser spot size/mm	0.2
Thickness of layer/mm	1
Laser absorptivity	0.95

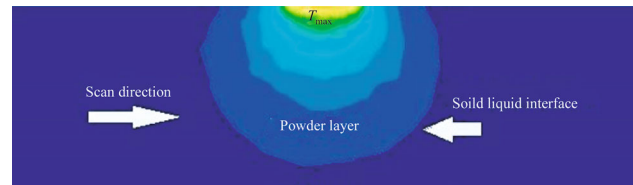


Fig. 2 Two-dimensional profile of Al-Si-10Mg powder in DMLS

$$G = \frac{T_{\max} - T_l}{r}, \quad (6)$$

where G is the temperature gradient, T_{\max} the maximum temperature in the melt pool, T_l the liquidus temperature of the alloy, r the distance between the liquidus line and the spot of the maximum temperature.

Based on the above calculation, the temperature gradient for a scan speed of 500 mm/s was found to be 528.27 K/mm and the phase-field profile at a different time during the sintering process is shown in Fig. 3. The phase-field simulations are carried out for liquid state sintering where the powder particles are first completely melted and then start to sinter. Thus, rapid melting and solidification behavior is observed during the process. The details of the thermal simulation and phase field modeling of a single particle are given elsewhere [27]. Initially, at time $t = 0$, a single seed having a radius of 10 μm is placed at the center of simulation domain. The color bar of the simulation domain represents the order parameter, and is dimensionless. In the color bar, “0” represents a completely liquid state and “100” represents a completely solid state. At $t = 50$ ms, the small particle starts evolving and forms a diamond structure as shown in Fig. 3a. In Fig. 3b, it is noticeable that the particle has started growing separately in all directions at $t = 300$ ms. At $t = 1\,500$ ms, the particle starts producing distinctive branches with constant temperature. From the simulation result, it is observed that with an increase in sintering time while maintaining a constant temperature gradient, the dendritic arms grow, and finally, the particle grows into a columnar structure. When the laser beam scans the powder bed, a large temperature gradient is created in the powder bed due to the high energy laser beam. This temperature

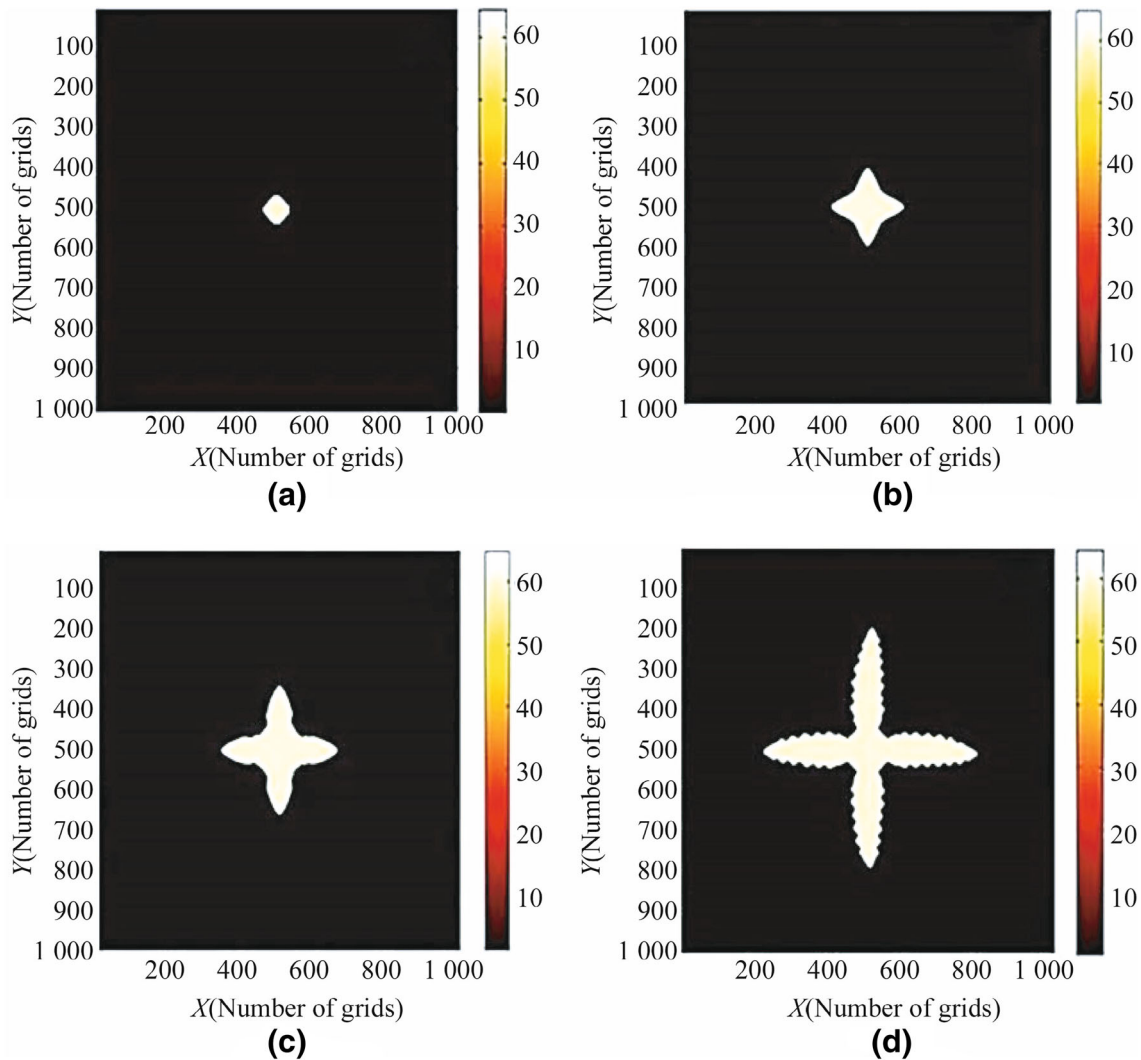


Fig. 3 Phase profiles of Al-Si-10Mg at different solidification time **a** $t = 50$ ms, **b** $t = 300$ ms, **c** $t = 1500$ ms, **d** $t = 13000$ ms

gradient helps to melt the powder particles in the bed, which then solidify and sinter within a few fractions of a second. Owing to the melting and solidification, a large temperature gradient exists in the powder bed, which encourages the growth of the dendritic arms.

4.1 Grain growth in multi-particle simulation at different sintering time

Phase field simulations of the microstructure evolution of Al-Si-10Mg were carried out by considering multiple seeds in the domain. The domain, seed size and all other features remain unchanged, except for the location of the seeds. There is one seed at the center and the remaining two seeds are placed nearby to study the grain growth behavior. The temperature gradient is used as the input parameter for the phase field simulation, which is calculated by using Eq. (6).

Taking the temperature gradient as 263.3 K/mm, the phase field profiles produced at different sintering times are shown in Fig. 4. This section exhibits the importance of different time steps and a constant temperature condition when examining the phase profiles. At the initial time step $t = 0$, the computational domain is initialized with multiple seeds as shown in Fig. 4a. Microstructural growth starts at 500 ms, when the grains start growing independently as shown in Fig. 4b. Figures 4c–e show the growth of the grains, which finally merge with each other, at 1500 ms, 4500 ms and 13000 ms, respectively. The grain boundaries appear to overlap with each other as time increases and the constant application of temperature causes the atoms to move faster. This is due to the cooling rate which varies with respect to time.

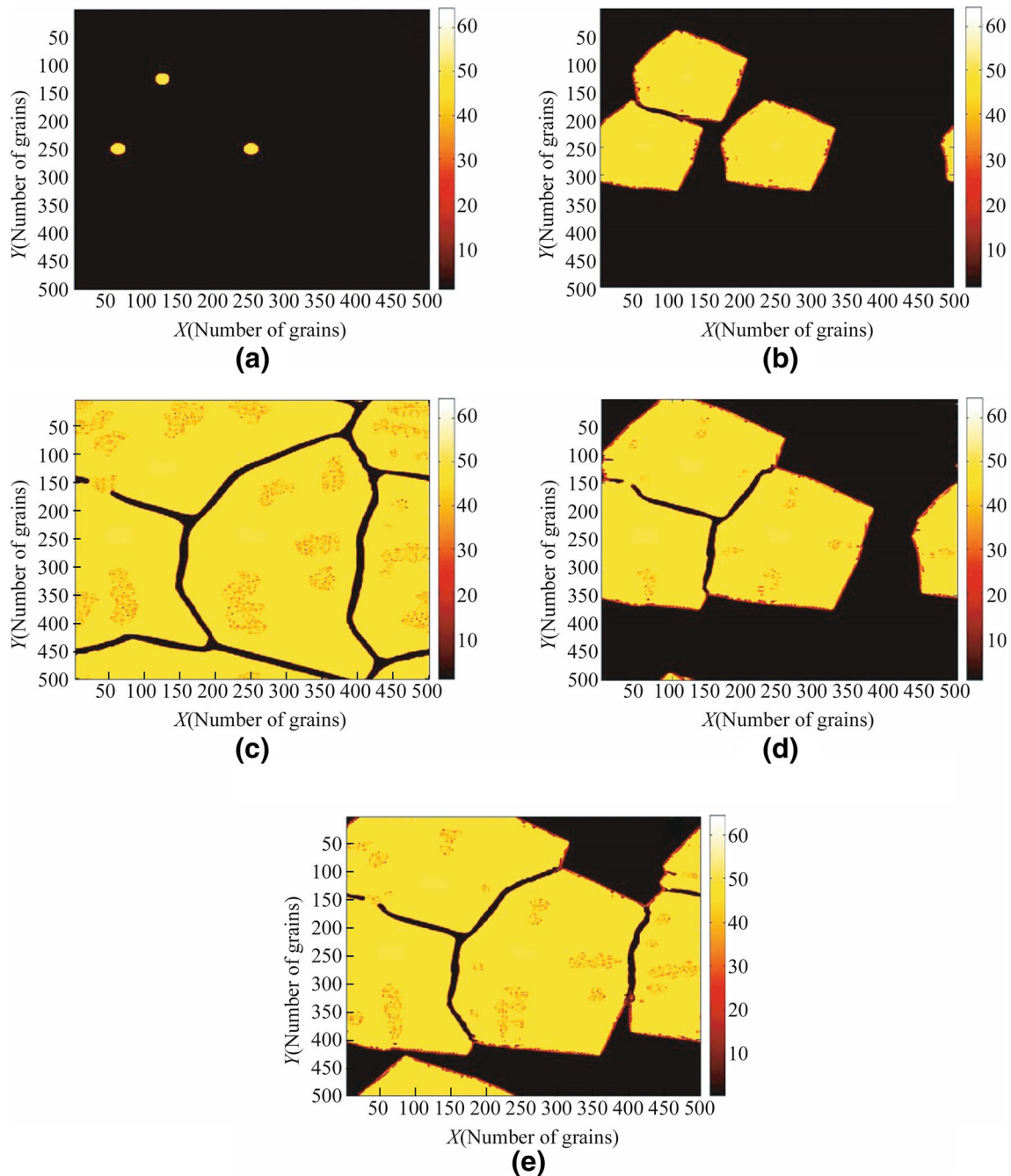


Fig. 4 Phase profiles of multiple Al-Si-10Mg particles at different solidification time **a** $t = 0$, **b** $t = 500$ ms, **c** $t = 1\,500$ ms, **d** $t = 4\,500$ ms, **e** $t = 13\,000$ ms

4.2 Grain growth of multi-particle simulation at different temperature gradients

As mentioned earlier, the temperature gradient plays a significant role in microstructure evolution. In the multi-particle domain, changes in the temperature gradient lead to grain growth in a different manner compared to that seen

in the single particle simulations. The temperature gradients used in this work are 263.3 K/mm, 318.18 K/mm, and 362.66 K/mm, which were calculated by using Eq. (6). Particle growth behavior has been studied using these temperature gradients at different time steps. Figure 5 shows the particle growth rate at $t = 500$ ms. It can be observed from Fig. 5 that the seeds grow independently,

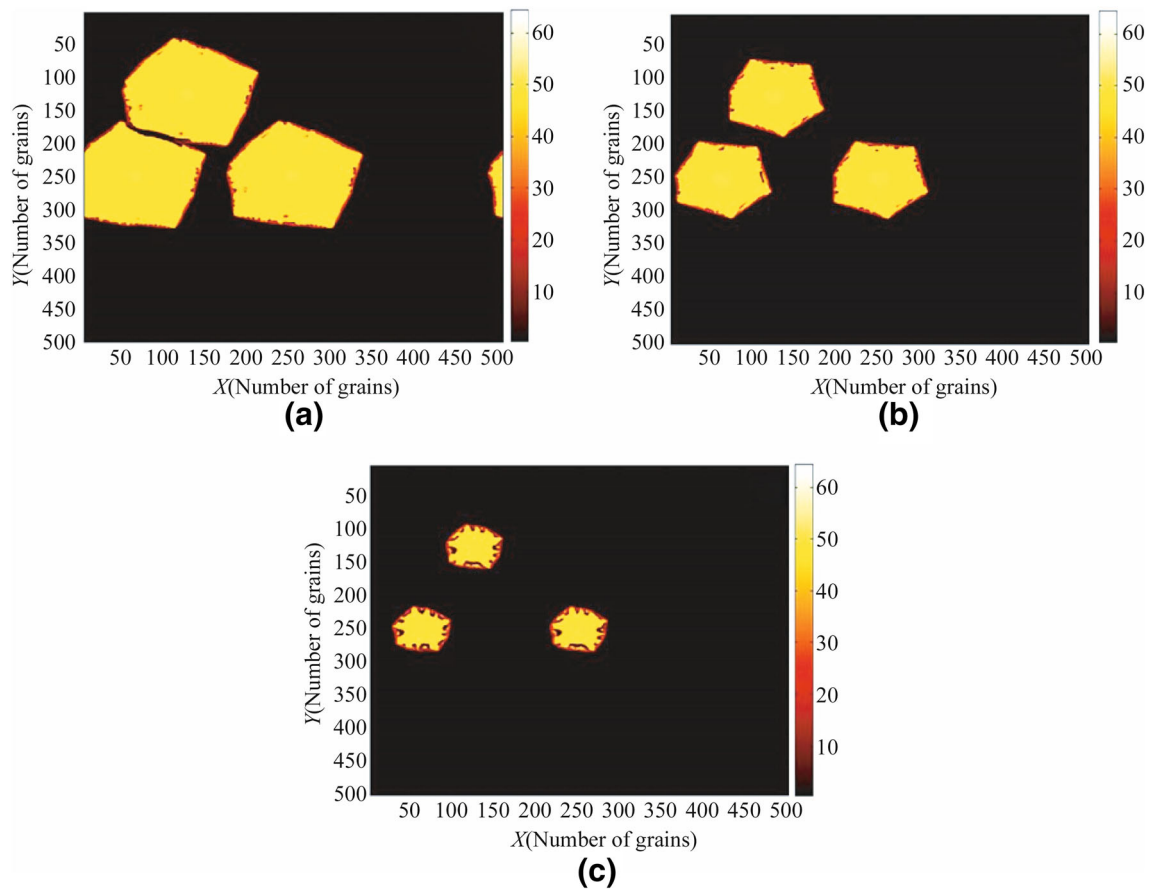


Fig. 5 Phase profiles of multiple Al-Si-10Mg particles at $t = 500$ ms with different temperature gradients **a** 263.33 K/mm, **b** 318.18 K/mm, **c** 362.66 K/mm

like single particles. Comparing temperature gradients of 263.33 K/mm, 318.18 K/mm, and 362.66 K/mm, Fig. 5c shows the finest grain structure as compared to Figs. 5a, b, owing to it having the highest temperature gradient. This can be attributed to the relationship between cooling rate and temperature gradient as given by Sahoo and Chou [17]

$$T = GS, \quad (7)$$

where T is the cooling rate, S the solidification growth rate.

Comparing Figs. 4 and 5, it seems that Fig. 5a is similar of Fig. 4b. Figure 4 shows the overall phase profile for temperature gradient 263.33 K/mm with respect to timesteps (263.33 K/mm has been chosen to show the overall phase profile). In that Fig. 4b is the one obtained at $t = 500$ ms. It seems similar to Fig. 5a because it shows the phase profile for temperature gradient 263.33 K/mm at $t = 500$ ms and the rest show the phase profiles for different temperature gradients at $t = 500$ ms (as a comparative study).

From Fig. 6, it is observed that the seeds grow and form dendritic tips with increasing sintering time ($t = 1500$ ms), and they finally start merging with the neighboring seed boundaries. Noticeably, from Fig. 6c, it can be concluded that at the highest temperature gradient, the grain boundaries have the most interaction. Gradually, with the increase in sintering time, the seeds grow larger in size, and form an interface instead of merging together. The parts that are not at the interface are seen to change shape due to a lower temperature gradient as compared to the interface, and they start filling the other parts of the domain. This is also clearly observed in Fig. 7 at different temperature gradients when the sintering time is 4500 ms.

Figure 8 shows the growth behavior of the Al-Si-10Mg seeds during the DMLS process, when the sintering occurs at $t = 13000$ ms. From the simulation results, it is observed that the seeds completely fill the domain by overpowering the interface and start merging fully. In Fig. 8a, sintering occurs at a lower rate due to a lower temperature gradient.

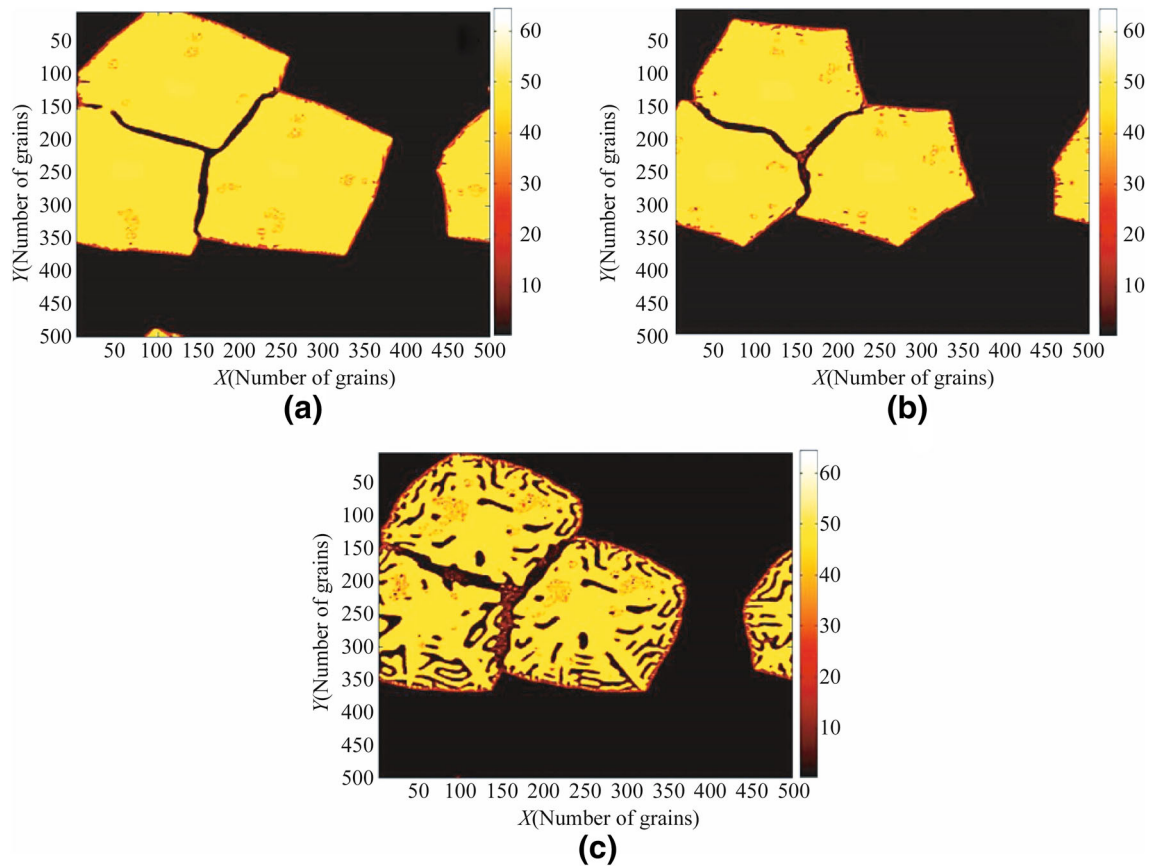


Fig. 6 Phase profiles of multiple Al-Si-10Mg particles at $t = 1\,500$ ms with different temperature gradients **a** 263.33 K/mm, **b** 318.18 K/mm, **c** 362.66 K/mm

As a result, the particles do not fully scatter over the domain. On the other hand, in Fig. 8b, sintering occurs partially, as there is better overlapping of the grain boundaries, along with the spreading of particles over the surface. Finally, Fig. 8c is seen to have the finest dendritic structures, and the higher temperature gradient results in the loss of free space in the domain.

By observing Figs. 7 and 8, both look same but both figures are at different time step. Figure 7 shows the phase profile at $t = 4\,500$ ms where the sintering and growth of microstructure has been completed. On the other hand, in Fig. 8, the time steps is increased to 13 000 ms to investigate if there is any change of microstructure occurring in the process. From the phase profile, it is found that there is no change occurring in the growth of microstructure after complete sintering. It may be occurred due to completion of diffusion of Si and Mg particles in Al matrix.

5 Conclusions

Simulations of the microstructure evolution of an Al-Si-10Mg alloy in a DMLS process were carried out using a phase-field method. Taking temperature gradient and laser scan speed as the process parameters, a MATLAB code was developed to solve the final phase-field equations. The temperature gradient was extracted from the molten pool in the thermal model. The simulations were applied to both single particle and multi-particle domains and the following observations were made:

- (i) In the single particle domain, the temperature gradient plays an important role in the solidification process along with the rapid growth rate of the seeds. It is also observed that the increase in the temperature gradients directly affects the microstructure evolution. The formation of dendrites increases with the increase in the temperature

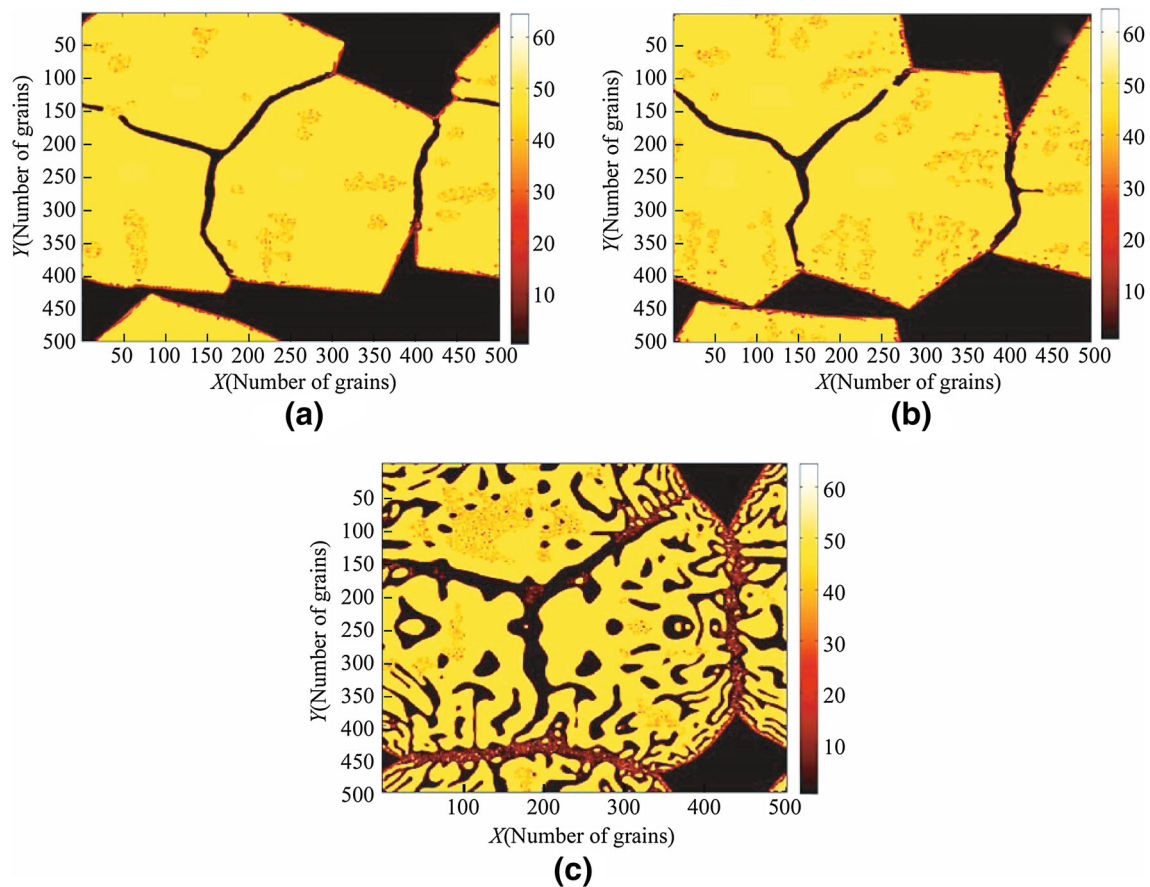


Fig. 7 Phase profiles of multiple Al-Si-10Mg particles at $t = 4\,500$ ms with different temperature gradients **a** 263.33 K/mm, **b** 318.18 K/mm, **c** 362.66 K/mm

gradient and the dendrite tips are observed to grow faster.

- (ii) In the multi-particle domain, it is observed that the grains grow in an independent manner owing to their arbitrary orientation, after which they coalesce, and impingement occurs between the closest grains. The increasing temperature gradients lead to the formation of finer dendrites initially, but with increasing time, the dendrites collide and grain growth are seen to be constrained at the

interface. The remaining parts other than the interface grow to fill the domain completely, subjected to lower temperature gradients. In addition, it is observed that the merging is better in the cases with the lowest and the highest temperature gradients, whereas in the case with an average gradient, it takes more time for the grains to completely merge with their surroundings, i.e., the solidification time required is larger compared to the other two cases.

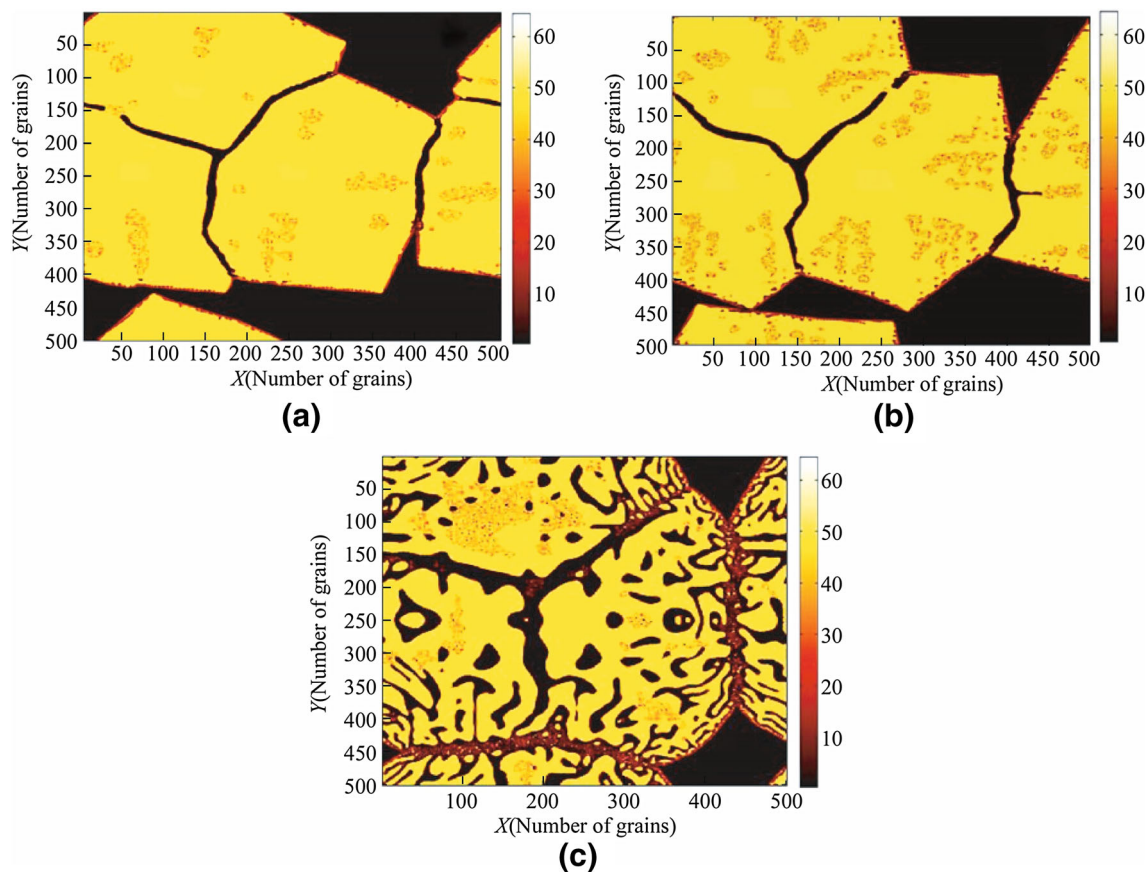


Fig. 8 Phase profiles of multiple Al-Si-10Mg particles at $t = 13\,000$ ms with different temperature gradients **a** 263.33 K/mm, **b** 318.18 K/mm, **c** 362.66 K/mm

References

- Noorani R (2006) Rapid prototyping: principles and applications. Wiley, London
- Chua CK, Chou SM, Lin SC et al (1998) Rapid prototyping assisted surgery planning. *Int J Adv Manuf Technol* 14(9): 624–630
- Kelly SM, Kampe SL (2004) Microstructural evolution in laser-deposited multilayer Ti-6Al-4V builds part I: microstructural characterization. *Metall Mater Trans* 35(6):1861–1867
- Brandl E, Baufeld B, Leyens C et al (2010) Additive manufactured Ti-6Al-4V using welding wire: comparison of laser and arc beam deposition and evaluation with respect to aerospace material specifications. *Phys Proc* 5:595–606
- Dinda GP, Song L, Mazumder J (2008) Fabrication of Ti-6Al-4V scaffolds by direct metal deposition. *Metall Mater Trans A* 39(12):2914–2922
- Thompson SM, Bian L, Shamsaei N et al (2015) An overview of direct laser deposition for additive manufacturing part I: transport phenomena, modeling and diagnostics. *Addit Manuf* 8:36–62
- Shamsaei N, Yadollahi A, Bian L et al (2015) An overview of direct laser deposition for additive manufacturing part II: mechanical behavior, process parameter optimization and control. *Addit Manuf* 8:12–35
- Cabrini M, Lorenzi S, Pastore T et al (2016) Evaluation of corrosion resistance of Al-10Si-Mg alloy obtained by means of direct metal laser sintering. *J Mater Process Technol* 231: 326–335
- Chen LQ (2002) Phase-field models for microstructure evolution. *Annu Rev Mater Res* 32(1):113–140
- Das P, Dutta P (2016) Phase field modeling of microstructure evolution and ripening driven grain growth during cooling slope processing of A356 Al alloy. *Comput Mater Sci* 125:8–19
- Du L, Zhang R (2014) Phase field simulation of dendrite growth with boundary heat flux. *Integr Mater Manuf Innov* 3(1):1–5
- Kazaryan A, Wang Y, Dregia SA et al (2000) Generalized phase-field model for computer simulation of grain growth in anisotropic systems. *Phys Rev B* 61(21):14275
- Mamivand M, Zaeem MA, El Kadiri H (2013) A review on phase field modeling of martensitic phase transformation. *Comput Mater Sci* 77:304–311
- Sciarra G (2016) Phase field modeling of partially saturated deformable porous media. *J Mech Phys Solids* 94:230–256
- Gránásy L, Pusztai T, Warren JA (2004) Modelling polycrystalline solidification using phase field theory. *J Phys Condens Matter* 16(41):R1205
- Ganeriwala R, Zohdi TI (2014) Multiphysics modeling and simulation of selective laser sintering manufacturing processes. *Proc CIRP* 14:299–304
- Sahoo S, Chou K (2016) Phase-field simulation of microstructure evolution of Ti-6Al-4V in electron beam additive manufacturing process. *Addit Manuf* 9:14–24
- Sahoo S (2014) Microstructure simulation of Ti-6Al-4V biomaterial produced by electron beam additive manufacturing process. *Int J Nano Biomater* 5(4):228–235
- Karma A (2001) Phase-field formulation for quantitative modeling of alloy solidification. *Phys Rev Lett* 87(11):115701

20. Tan W, Bailey NS, Shin YC (2011) A novel integrated model combining cellular automata and phase field methods for microstructure evolution during solidification of multi-component and multi-phase alloys. *Comput Mater Sci* 50(9):2573–2585
21. Fallah V, Amoozrezaei M, Provatas N et al (2012) Phase-field simulation of solidification morphology in laser powder deposition of Ti-Nb alloys. *Acta Mater* 60(4):1633–1646
22. Gong X, Chou K (2015) Phase-field modeling of microstructure evolution in electron beam additive manufacturing. *JOM* 67(5):1176–1182
23. Biswas S, Schwen D, Singh J et al (2016) A study of the evolution of microstructure and consolidation kinetics during sintering using a phase field modeling based approach. *Extreme Mech Lett* 7:78–89
24. Holfelder P, Lu JM, Kremaszky C et al (2016) A phase field approach for modeling melting and re-solidification of Ti-6Al-4V during selective laser melting. *Key Eng Mater* 704:241–250
25. Hang K, Mastorakos I (2017) Phase field crystal simulation of grain growth in BCC metals during additive manufacturing. *MRS Adv* 2(16):887–896
26. Kundin J, Mushongera L, Emmerich H (2015) Phase-field modeling of microstructure formation during rapid solidification in Inconel 718 super alloy. *Acta Mater* 95:343–356
27. Nandy J, Sarangi H, Sahoo S (2017) Modeling of microstructure evolution in direct metal laser sintering: a phase field approach. *Mater Sci Eng* 178:1–8